

Accepted Manuscript

In vitro and *in vivo* characterization of a novel, highly potent p53-MDM2 inhibitor

Andrea Vaupel, Philipp Holzer, Stephane Ferretti, Vito Guagnano, Joerg Kallen, Robert Mah, Keiichi Masuya, Stephan Ruetz, Caroline Rynn, Achim Schlapbach, Thérèse Stachyra, Stefan Stutz, Milen Todorov, Sébastien Jeay, Pascal Furet

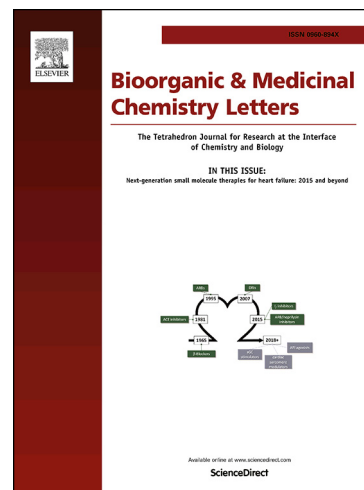
PII: S0960-894X(18)30703-0
DOI: <https://doi.org/10.1016/j.bmcl.2018.08.027>
Reference: BMCL 26007

To appear in: *Bioorganic & Medicinal Chemistry Letters*

Received Date: 28 June 2018
Revised Date: 18 August 2018
Accepted Date: 24 August 2018

Please cite this article as: Vaupel, A., Holzer, P., Ferretti, S., Guagnano, V., Kallen, J., Mah, R., Masuya, K., Ruetz, S., Rynn, C., Schlapbach, A., Stachyra, T., Stutz, S., Todorov, M., Jeay, S., Furet, P., *In vitro* and *in vivo* characterization of a novel, highly potent p53-MDM2 inhibitor, *Bioorganic & Medicinal Chemistry Letters* (2018), doi: <https://doi.org/10.1016/j.bmcl.2018.08.027>

This is a PDF file of an unedited manuscript that has been accepted for publication. As a service to our customers we are providing this early version of the manuscript. The manuscript will undergo copyediting, typesetting, and review of the resulting proof before it is published in its final form. Please note that during the production process errors may be discovered which could affect the content, and all legal disclaimers that apply to the journal pertain.



In vitro and *in vivo* characterization of a novel, highly potent p53-MDM2 inhibitor

Andrea Vaupel*, Philipp Holzer, Stephane Ferretti, Vito Guagnano, Joerg Kallen, Robert Mah, Keiichi Masuya^a, Stephan Ruetz, Caroline Rynn^b, Achim Schlapbach, Thérèse Stachyra, Stefan Stutz, Milen Todorov, Sébastien Jeay^c and Pascal Furet

Novartis Institutes for BioMedical Research, CH-4002 Basel, Switzerland

^a present address: Peptidream Inc.; Menguro Tokyo, Japan

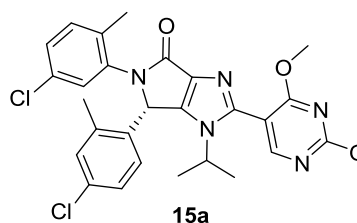
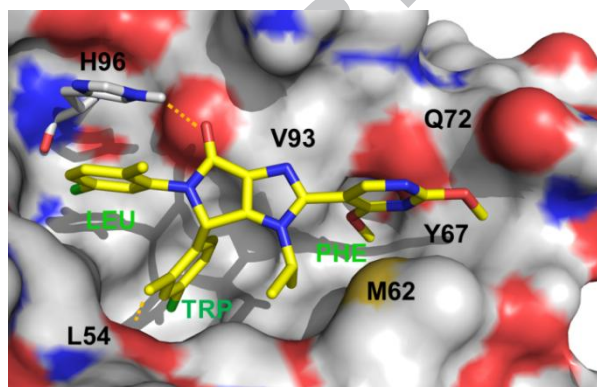
^b present address: Hoffmann-LaRoche; CH-4070, Basel, Switzerland

^c present address: Idorsia Pharmaceuticals; CH-4123 Allschwil, Switzerland

Abstract

Small molecule inhibitors of the p53-MDM2 protein complex are under intense investigation in clinical trials as anti-cancer agents, including our first generation inhibitor NVP-CGM097. We recently described the rational design of a novel pyrazolopyrrolidinone core as a new lead structure and now we report on the synthesis and optimization of this to provide a highly potent lead compound. This new compound displayed excellent oral efficacy in our preclinical mechanistic *in vivo* model and marked a significant milestone towards the identification of our second generation clinical candidate NVP-HDM201.

Graphical abstract



15a
80 pM IC₅₀ MDM2 TR-FRET
11 nM GI₅₀ SJSA1 cell proliferation

Key words

HDM201; structure guided design; X-ray structure; MDM2-p53 protein-protein interaction (PPI) inhibitors; pyrrolo[3,4-d]imidazol-4(1H)-ones

The p53 protein functions as a transcription factor capable of regulating a number of genes driving the cell cycle and apoptosis. As such it acts as a tumor suppressor, helping to control cellular integrity and prevent the proliferation of permanently damaged cells by initiating growth arrest or cell death.¹ Under non-stressed conditions these activities are tightly controlled through negative regulation by the MDM2 (also known as HDM2 as the human homolog) protein. MDM2 has a dual function by inhibiting p53 transcriptional activity and by mediating the ubiquitin-dependent degradation of p53. About 50% of human cancers express wild type (wt) functional p53 protein and avoid its tumor suppressor function by overexpression of MDM2. In many other tumors the protective role of p53 is abrogated by expression of loss of function mutations. As a consequence, selective disruption of the p53-MDM2 interaction in cancer cells expressing wt p53 could serve as a valuable therapeutic strategy to inhibit tumor growth.

The X-ray structure of the *N*-terminal domain of MDM2 bound to a 15-mer wt p53-derived peptide was reported over 20 years ago and revealed three discrete sub-pockets in the binding site. These pockets are occupied by three amino acid side chains from p53 (Phe 19, Trp 23, Leu 26)² which are conserved across species.³ This structural information paved the way for the discovery of several structurally distinct small molecule inhibitors of this protein-protein interaction (PPI). Several of these progressed into clinical trials for evaluation as treatments of hematological as well as solid tumors. The most advanced agent, Indasanutlin, is currently being investigated in Phase III studies in combination with Cytarabine.⁴

Shortly after the first publication of the X-ray structure of the p53/MDM2 complex our group initiated work around p53-derived peptides to provide an initial insight into the key SAR for this PPI.⁵ We then proceeded to develop a new, pocket-adapted scaffold approach for the *de novo* design of small molecule MDM2 inhibitors, which we termed the central valine concept.⁶ This was based upon the observation that the side chain of valine 93 of MDM2 occupied the central upper-part of the p53 binding pocket and could serve as an ideal anchor point for a tight van der Waals interaction with an aromatic or hetero-aromatic core of a ligand molecule. Such a core would provide appropriate exit vectors for substituents to interact with the Phe19, Leu26 and Trp23 sub-pockets of the binding cavity. In utilizing this principle we identified several generations of highly potent MDM2 ligands including the isoquinolinone series from which we identified the clinical candidate NVP-CGM097.⁷

In subsequent refinements of the central valine concept we described the design of a new, bicyclic pyrazole-based ligand scaffold.⁸ As a continuation, we now report on the chemical synthesis and the further optimization of this new MDM2 inhibitor class towards a highly potent lead compound displaying excellent *in vivo* efficacy and pharmacokinetic properties in our preclinical SJSA1 tumor model upon oral administration.

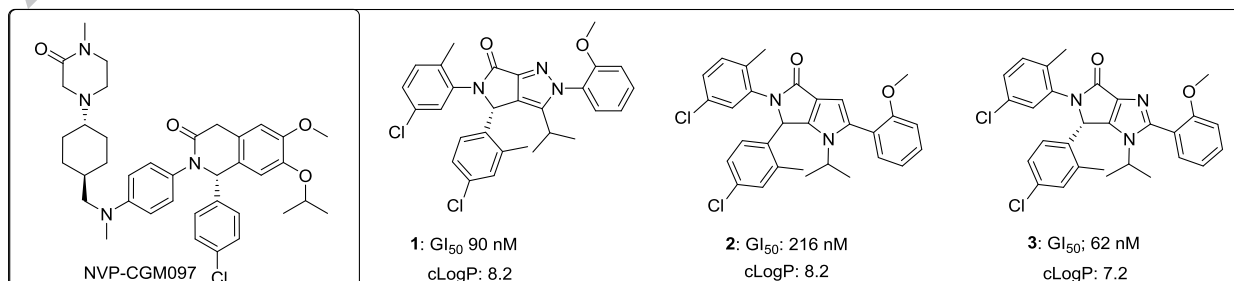


Figure 1: Chemical structure of NVP-CGM097 and scaffold permutations of compound **1**. Antiproliferative activities in SJSA1 cells is indicated by GI₅₀ values and compound lipophilicity is indicated by calculated LogP values

The starting point for this work is represented by the pyrazolo-pyrrolidinone compound **1**. Compound **1** is a highly potent inhibitor of the p53-MDM2 interaction in our biochemical TR-FRET assay (IC₅₀: 0.13 nM)⁹ and a proliferation assay based on p53 wt SJSA1 cells (GI₅₀: 90 nM).¹⁰ The X-ray structure of a close analog of **1** complexed with MDM2 has been reported⁸ and confirmed our postulated binding mode. It demonstrated that the bicyclic core unit indeed is in close van der Waals contact with the side-chain of V93, while accepting an H-bond from the side chain of H96 via the lactam carbonyl. As expected, the chloro-phenyl moieties occupy the Trp23 and Leu26 pockets and, in the latter, the phenyl ring engages in a π - π stacking interaction with H96. In addition it confirmed the reason for the significant potency increase observed in early SAR, when we attached a phenyl moiety on the lactam nitrogen, allowing the ligand to occupy the extended Phe19 pocket. In particular an ortho-methoxy substituent in such a phenyl ring further contributes to a favorable pre-organization of the ligand and topological fit within the binding cavity. Despite the combination of high on-target potency and low molecular weight, compound **1** displayed some liabilities as a potential drug candidate. The high, cross species metabolic clearance (Cl_{int} [mL/min mg] rat/human/mouse: 385/115/495), as determined by incubation with liver microsomes, precluded its suitability as an in vivo tool compound for proof-of-concept studies of this new inhibitor class. Therefore our first optimization cycle aimed to overcome this hurdle. Upon morphing the pyrazole compound **1** to the pyrrole (compound **2**) or the imidazole (compound **3**), with the peripheral substitution pattern being kept constant (Figure 1), we observed that such permutations were tolerated with the intrinsic potency being retained. The imidazole core seemed to offer advantages in reducing lipophilicity (clogP values) as compared to pyrazoles and pyrroles and hence we directed our focus for optimization on the imidazole core unit.

Conducting a Metasite^{*11} analysis of compound **3** inferred that the methoxy-phenyl moiety filling the Phe19 pocket was a major contributor to the high metabolic clearance, due to its susceptibility for oxidative metabolism. In order to address this we sought to reduce electron density by adding appropriate substituents to the aromatic core or by incorporating nitrogen atoms.

Thus, we prepared a series of compounds based on the imidazole scaffold with representative examples shown in Table 1.

The general synthetic route employed to prepare these compounds is depicted in Scheme 1.¹² Starting with the condensation of commercially available ethyl 2-isocyanoacetate with N,N-dimethylformamide-diethylacetal followed by reaction of the intermediate ethyl (Z)-3-(dimethylamino)-2-isocyanoacrylate with isopropylamine in n-butanol at 70°C provided ethyl 1-isopropyl-1H-imidazole-4-carboxylate **4** in good yield. **4** was directly subjected to bromination with NBS at room temperature to afford a mixture of the desired ethyl 2-bromo-1-isopropyl-1H-imidazole-4-carboxylate **5** and its regioisomer, ethyl 5-bromo-1-isopropyl-1H-imidazole-4-carboxylate, which was readily separated by flash chromatography on silica gel. Lithiation at C-5 and quenching with 4-chloro-2-methylbenzaldehyde produced the alcohol **6**, which was converted to the corresponding mesylate and reacted with 5-chloro-2-methylaniline to provide

intermediate **7**. The ester functionality of **7** was hydrolyzed to the acid and converted to the corresponding acid chloride by treatment with Ghosez's reagent (1-chloro-N,N-2-trimethyl-1-propenylamine) leading to efficient ring-closure to produce the bicyclic lactam scaffold of intermediate **9**. The 2-bromo imidazole finally served as a template for Suzuki cross coupling reactions with commercially available boronic acids to provide compounds **10-15**.

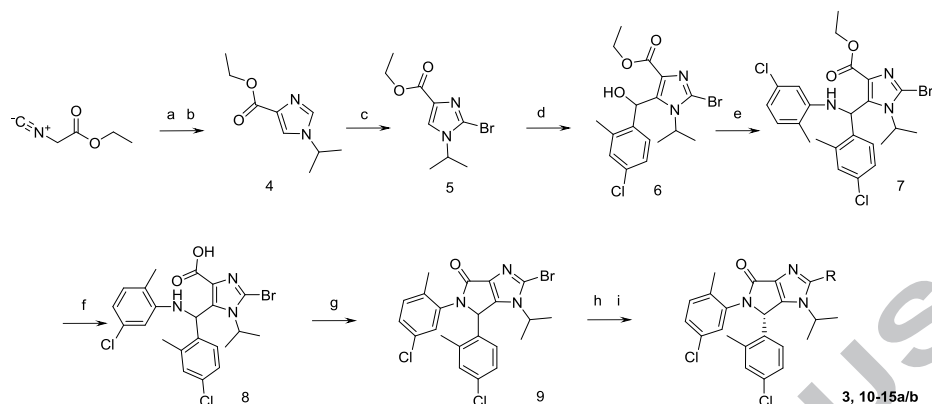
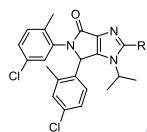


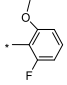
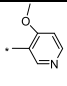
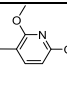
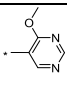
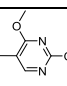
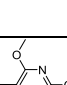
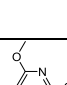
Figure 2: Representative synthesis; conditions a) *N,N*-dimethylformamide-diethylacetal, EtOH, 0-25°C/4h; 75%; b) *i*-PrNH₂, *n*-BuOH; 70°C/24h; 85%; c) NBS, THF, 16h/rt; 36%; d) *n*-BuLi, DIPA, 2-methyl-4-chlorobenzaldehyde, THF, 1.5h, -65°C to rt; 71%; e) i) Ms₂O, Et₃N, DCM; ii) 5-chloro-2-methylaniline; 78%; f) 2M NaOH, THF/MeOH, 4h, rt; 88%; g) Ghosez's reagent, DCM, 1h, 0°C; 88%; h) Pd(dppf)Cl₂, K₃PO₄, ArylB(OH)₂, dioxane/H₂O 4:1, 2h, 85°C; 84%; i) chiral separation; 41%. Representative yields are given for the synthesis of compound **15a**.

Selected racemic products of special interest were then subjected to chiral chromatography for further profiling of the more active enantiomer.

Table 1. Comparison of selected properties of analogs of compound **3**



compound	Structure R	MDM2 IC ₅₀ (nM)**	TR-FRET	GI ₅₀ SJS1 cell (nM)	RLM Cl (mL/min mg)	T ½ (min)
3 S-enant		0.074		64 **	385	3.6
10 rac		0.14		228 ± 25	460	3.3

11 rac		0.17	276 ± 46	450	3.3
12 S-enant		0.26	345 ± 41	117	12
13 rac		0.22	186*	69	20
14 rac		0.26	111 ± 20	178	8
15 rac		0.16	26 ± 5	47	30
15 a S-enant		0.08	11 ± 3	35	39
15 b R-enant		13	1001 ± 166	25	56

*single determination; ** data is an average of more than two independent measurements; rac: racemic mixture

The direct incorporation of fluorine atoms into the aromatic ring in an attempt to reduce oxidative clearance is exemplified by racemic examples compounds **10** and **11**. However, this modification did not have a positive impact on in vitro RLM clearance, our primary reference parameter (Table 1). We probed the effect of incorporating ring nitrogen atoms in combination with the 2-methoxy substituent in various combinations, as exemplified with compounds **12**, **13** and **14** and to our delight observed a positive trend towards improved metabolic stability. The most favorable combination of reduced in vitro clearance and significantly enhanced potency compared to our starting point was obtained with 2,4-dimethoxy pyrimidine compound **15**. Compound **15** was selected as a lead compound from that set for chiral separation by reversed phase chromatography providing the more potent S-enantiomer **15a** and the less active R-enantiomer **15b**. The S-enantiomer **15a** displayed favorable in vitro properties with good metabolic stability across species in liver microsomal incubations (Cl_{int} [mL/min mg] r/h/m/d/monkey: 35/72/36/35/20), half-lives (r/h/m/d/monkey: 39/17/39/40/81 min), as well as high passive permeability in PAMPA assays (calc. FA: 99 %).

To investigate the potential activity of compound **15a** in preclinical tumor models, we evaluated the anti-proliferative activity of **15a** against a panel of 405 cell lines from the Cancer Cell Line Encyclopedia (CCLE).¹³ Cell lines were partitioned into sensitive and insensitive groups based on compound anti-proliferative effects (IC_{50}). A waterfall plot of IC_{50} values for **15a** showed a natural cut-off of 4 μ M, which was used to categorize cell lines (**Figure 4**). One hundred and three cell lines (25.4%) were categorized as

sensitive and 302 cell lines (74.6%) as insensitive. As expected, consistent with the expected mechanism of action of compound **15a**, most of the sensitive cell lines express wt p53 (96/103; 93.2%), strongly suggesting that wt p53 status is a prerequisite for the anti-proliferative activity of **15a**.

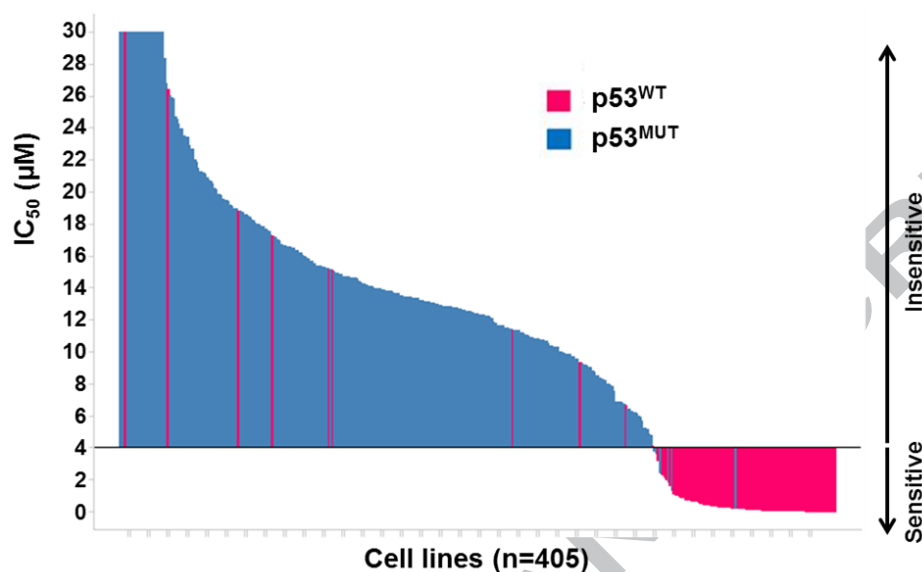


Figure 4: Waterfall plot showing IC₅₀ values expressed in μM of compound **15a** in cell viability assays. Data for wt p53 (p53^{WT}) cells are in pink and for mutant p53 (p53^{MUT}) cell lines in blue.

Co-crystallization experiments of racemic compound **15** with a truncated form of the human MDM2 protein confirmed that only the *S*-enantiomer formed stable complexes. The X-ray structure of the co-crystal of **15a** at 2.0 Å resolution (Figure 3) shows that the dihydropyrrolo-imidazole core binds MDM2 in an identical mode to that observed for the dihydropyrrolo-pyrazole core (pdb code 5LN2). In particular, the dihydropyrrolo-imidazole core of the compound makes van der Waals contacts with the central MDM2 residue V93 and the pyrrolo-oxygen accepts an H-bond (3.1 Å) from the side-chain of H96. The chloro-phenyl moieties occupy the Trp 23 and Leu 19 sub-pockets. In the Leu19 sub-pocket we once more observed the π - π stacking interaction with H96. The 2-methyl in the Trp23 sub-pocket donates a pseudo H-bond (3.0 Å) to the backbone-carbonyl of Leu54. The Phe19 sub-pocket is occupied by the 2,4-dimethoxypyrimidine moiety, where the 4-methoxy group fits snugly into a small cavity located beneath the backbone-carbonyl of Q72, as previously observed in the crystal structure of MDM2 in complex with an analog of **1**.^{7,8} The additional 2-methoxy-substituent present in compound **15** engages in favorable van der Waals interactions with the side-chains of residues M62, Y67 and Q72 of the MDM2 protein. This observation is consistent with the increased potency observed for **15** when compared to its des-methoxy analog compound **14**.

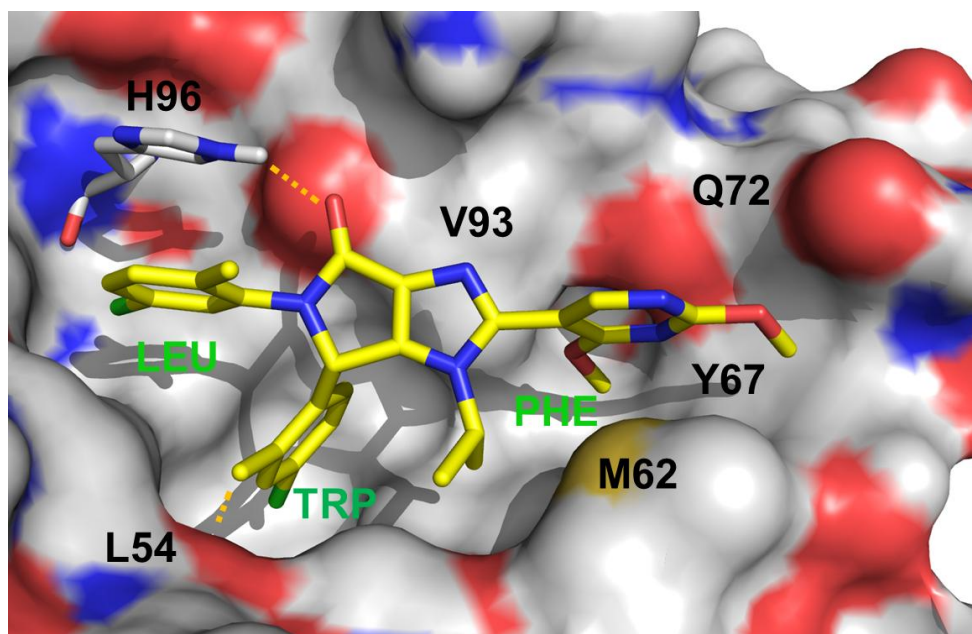


Figure 3. Crystal structure of MDM2 in complex with compound **15a** (pdb code: 6GGN). The direct H-bond is indicated with a dashed line. The MDM2 sub-pockets binding the p53 residues Leu 26, Trp 23 and Phe 19 are labeled LEU, TRP and PHE respectively.

For *in vivo* characterization we performed low dose PK studies of compound **15a** in male Sprague Dawley rats. The compound was administered by both intravenous (i.v.) and oral (p.o.) routes. For i.v. administration a dose of 1 mg/kg was given as a solution formulation (NMP/PEG 70:30), whereas the oral dose of 3 mg/kg was applied as suspension (carboxymethylcellulose/ water/ Tween80, (0.5%/ 99%/ 0.5%). The compound displayed a moderate total clearance of 50% of the rat hepatic blood flow (70 ml/min/kg) and a robust C_{max} of 75 nM (d. n.) with a half life ($T_{1/2}$) of 1.8 h and a good oral bioavailability (F) of 67% (Table 2). Taken together the data indicated that **15a** was suitable candidate for *in vivo* proof of concept studies in our preclinical mechanistic human SJSA1-based xenograft model in immunodeficient rats.

Table2: Pharmacokinetic data for compound **15a**

CL (i.v.) (mL·min ⁻¹ ·kg ⁻¹)	$T_{1/2}$ (i.v.) (h)	Vss (i.v.) (l·kg ⁻¹)	AUC (i.v.) (nM·h d.n.)	AUC (p.o.) (nM·h d.n.)	Cmax (p.o.) (nmol d.n.)	T max (p.o.) (h)	F (%) (calculated)
32 ± 14	1.8 ± 0.2	4.4 ± 1.1	1080 ± 15	719 ± 165	75 ± 3	2 ± 0	67 ± 15

^a intravenous (i.v.) dose provided as solution formulation in NMP/PEG (70/30) 1 mg/kg and 3 mg /kg p.o. as a suspension in Tween 80 / CMC05/ water (0.5/0.5/99) 3 mg/kg; d.n. : dose normalized

For the evaluation of *in vivo* efficacy SJSA-1 tumor cells were injected subcutaneously into the right flank of nude rats. 14 days after injection tumors had reached an average volume of 500 mm². Treatment was initiated by randomizing animals according to tumor size into a vehicle control group and three treatment groups (n=6 for all groups), with compound **15a** being administered orally at 1 mg, 3 mg or 5

mg/kg once daily (qd). The compound dose-dependently reduced tumor growth and was well tolerated at all doses (Figure 5A). Tumor volume was reduced by 40% at 1 mg/kg and statistically significant tumor regression was observed with 3 and 5 mg/kg doses (32% and 98% respectively) after 14 days of treatment (Figure 5A). The total body weight increase of treated animals was comparable to that of vehicle-treated animals (Figure 5B). The oral absorption of **15a** was dose-dependent with the same plasma profile at all three doses evaluated. The C_{max} of **15a** was reached after three hours and clearance to very low levels was seen within 24h. In order to investigate the pharmacokinetics (PK) in relation to representative pharmacodynamic (PD) markers for **15a**, we focused on the total drug concentration in plasma and analyzed upregulation of the mRNA expression of three p53 regulated target genes in tumor: p21, PUMA and MDM2 (Figure 5C). The treatment of SJSA-1 tumor-bearing rats with 1 and 3 mg/kg of **15a** showed a dose-dependent induction of the three p53 target genes in the tumor, reaching the maximum effect (E_{max}) for p21, PUMA and MDM2 during 3 to 8 hours post-treatment. However, mRNA induction remained relatively moderate for PUMA and MDM2 (E_{max} = 6- and 7-fold respectively), but high for p21 (E_{max} = 14-fold). Overall the observed changes in PD for the 1 and 3 mg dosing groups correlated well with the impact on tumor growth. Tumor PD analysis for the 5 mg dosing group was not feasible due to the lack of tumor tissue after treatment.

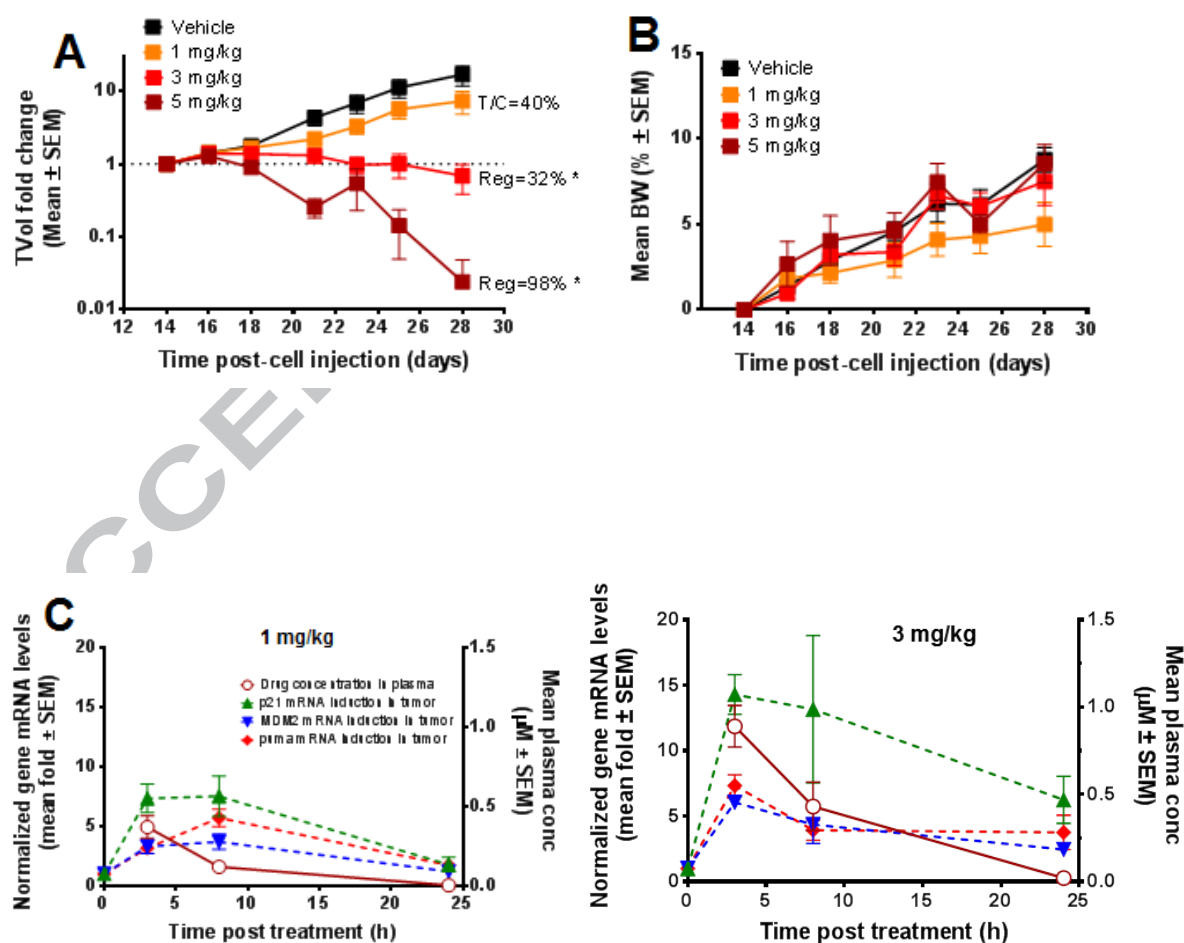


Figure 5: *In vivo* efficacy of compound **15a**: upper panel: left: A) impact on tumor volume (TVol); right: B) impact on mean bodyweight change (BW) for each dosing cohort over time; lower panel: C) mRNA levels of PD markers determined by quality reverse transcription PCR: p21 (green); MDM2 (blue); PUMA (red) and plasma exposure of drug substance (brown); left chart: 1 mg/timepoints post last dose; right chart: 3 mg/time points post last dose

Herein we have detailed the synthesis and biological activity of a novel MDM2 inhibitor. The new scaffold was designed based upon our pocket-adapted scaffold approach by iteratively incorporating sequential learning cycles from previous generations of inhibitors. This resulted in a highly optimized core scaffold with optimal complementarity to the binding pocket topology as demonstrated in our X-ray study. In this first optimization cycle our lead structure was elaborated to afford a tool compound, **15a**, suitable for *in vivo* proof of concept studies. Compound **15a** was highly efficacious in our mechanistic SJSA1 tumor model and well tolerated without impact on bodyweight after two weeks of continuous qd administration. This data compares favorably with those obtained for our first clinical candidate NVP-CGM097⁷, demonstrating the potential of the new lead series to provide superior clinical candidates. The continuation of this optimization towards the second generation clinical development candidate NVP-HDM201¹⁴ will be reported in a forthcoming publication.

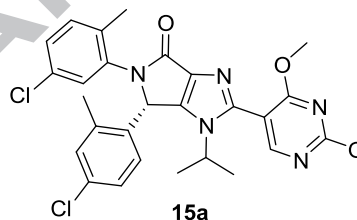
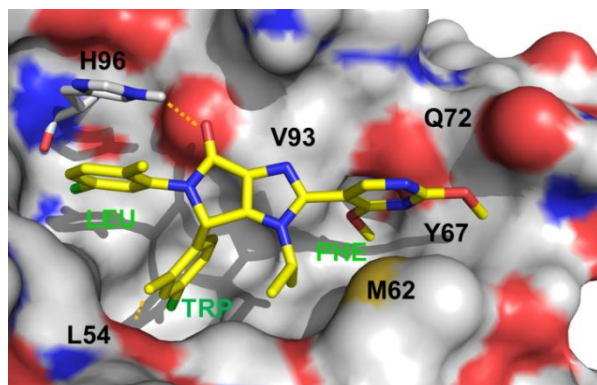
References:

1. For recent reviews on the topic see: (a) Burgess, A.; Chia, K. M.; Haupt, D.; Thomas, D.; Haupt, Y.; Lim, E. *Frontiers in Oncology* **2016**, *6*, article 7. (b) Zhao, Y.; Aguilar, A.; Bernard, D.; Wang, S. *J. Med. Chem.* **2015**, *58*, 1038. (c) Lv, P. -C.; Sun, J. Zhu, H. -L. *Curr. Med. Chem.* **2015**, *22*, 618. (d) Hoe, K. K.; Verma, C. S.; Lane, D. P. *Nat. Rev. Drug. Discov.* **2014**, *13*, 217. (e) Nag, S.; Zhang, X.; Srivenugopal, K. S.; Wang, M. -H.; Wang, W. Zhang, R. *Curr. Med. Chem.* **2014**, *21*, 553. (f) Wade, M.; Li, Y. C.; Wahl, G. M. *Nature Rev. Cancer* **2013**, *13*, 83. (g) Li, Q.; Lozano, G. *Clin. Cancer Res.* **2013**, *19*, 34.
2. To avoid confusion the one letter code is used to name the amino acid residues of MDM2 while the three letter code is used for those of p53.
3. Kussie, P. H.; Gorina, S.; Marechal, V.; Elenbaas, B.; Moreau, J.; Levine, A. J.; Pavletich, N.P. *Science* **1996**, *274*, 948.
4. <https://clinicaltrials.gov/>
5. García-Echeverría, C.; Chène, P.; Blommers, M.; Furet P. *J. Med. Chem.* **2000**, *43*, 3205.
6. Furet, P.; Chène, P.; De Pover, A.; Stachyra-Valat, T.; Hergovich Lisztwan, J.; Kallen, J.; Masuya, K. *Bioorg. Med. Chem. Lett.* **2012**, *22*, 3498
7. Holzer, P.; Masuya k.; Furet, P.; Kallen J.; Valat-Stachyra, T.; Ferretti, S.; Berghausen, J.; Bouisset-

- Leonard, M.; Buschmann, N.; Pissot-Soldermann, C.; Rynn, C.; Ruetz, S.; Stutz, S.; Chene, P.; Jeay, S.; Gessier, F. *J. Med. Chem.* **2015**, *58*, 6348.
8. Furet, P.; Masuya, K.; Kallen, J.; Stachyra-Valat, T.; Ruetz, S.; Guagnano, V.; Holzer, P.; Mah, R.; Stutz, S.; Vaupel, A.; Chène, P.; Jeay, S.; Schlapbach, A. *Bioorg. Med. Chem. Lett.* **2016**, *26*, 4837.
 9. For a detailed description of the TR-FRET (Time Resolved Fluorescence Resonance Energy Transfer) biochemical assay used see: Furet, P.; Guagnano, V.; Holzer, P.; Kallen, J.; Liao, L.; Mah, R.; Mao, L.; Masuya, K.; Schlapbach, A.; Stutz, S.; Vaupel, A. PCT Int. Appl. WO 2013111105. In this assay the donor fluorophore is MDM2 (amino acid residues 2-188) tagged with a C-terminal biotin moiety in combination with a Europium labeled streptavidin. The acceptor fluorophore is a p53 derived peptide (amino acid sequence 18-26 of p53: TFSDLWKLL) labeled with the fluorescent dye Cy5. For reference, the p53-MDM2 inhibitor Nutlin-3a has an IC_{50} of 0.01 μ M in this assay.
 10. Our cellular assay measures the ability of compounds to inhibit the proliferation of SJSA-1 cells. These are p53 positive cancer cells in which the MDM2 gene is amplified. For control, inhibition of the proliferation of the p53-null SAOS-2 cells is also measured. A detailed description of the cellular SJSA-1 and SAOS-2 proliferation assays is given in: Furet, P.; Guagnano, V.; Holzer, P.; Kallen, J.; Liao, L.; Mah, R.; Mao, L.; Masuya, K.; Schlapbach, A.; Stutz, S.; Vaupel, A. PCT Int. Appl. WO 2013111105. Usually, at least two orders of magnitudes in potency are lost going from a biochemical to a cellular setting. As the consequence of the p53-MDM2 auto-regulatory loop existing in cells, the accumulation of p53 caused by the inhibitors triggers an increase of cellular MDM2 levels which reduces inhibitor potency. See for example: Lahav G. In *Cellular Oscillatory Mechanisms*; Maroto, M.; Monk, N. A. M., Eds; Landes Bioscience and Springer Science, **2008**, pp 28-38. The fact that in cells, the inhibitors compete with full length p53 instead of the truncated form used in the biochemical assay is also likely to contribute to this loss of potency.
 11. Trunzer, M.; Faller, B.; Zimmerlin, A. *J. Med. Chem.* **2009**, *52*, 329.
 12. For detailed descriptions of experimental procedures and conditions refer to WO2013111105.
 13. a) Barrentina, J.; Capongro, G.; Stransky, N.; Venkatesan, K.; Margolin, A. A.; Morresey, M.P.; Sellers, W.; Schlegel, R.; Garraway, L. A. *et. al. Nature* **2012**, *483*, 603. b) McDonald III, E.R.; de Weck, A.; Schlabach, M.R.; Billy, E.; Mavrakis, K.J.; Hoffman, G.R.; *et al. Cell* **2017**, *170*(3), 577.
 14. a) Holzer, P.; Chene, P.; Ferretti, S. R.; Furet, P.; Gabriel, T.; Gruenenfelder, B.; Guagnano, V.; Hofmann, F.; Kallen, J. Mah, R.; Masuya, K.; Ramos, R.; Ruetz, S.; Rynn, C.; Schlapbach, A.; Valat, T.-M.; Stutz, S; Vaupel, A.; Jeay, S. (2016) [*Discovery of NVP-HDM201 - First disclosure of a Next-Generation Mdm2 inhibitor with superior characteristics.*](#) In: Annual Meeting of the AACR, 16-21 April, New Orleans, LA, USA. b) Holzer, P.; Chene, P.; Ferretti, S. R.; Furet, P.; Gabriel, T.;

Gruenenfelder, B.; Guagnano, V.; Hofmann, F.; Kallen, J. Mah, R.; Masuya, K.; Ramos, R.; Ruetz, S.; Rynn, C.; Schlapbach, A.; Valat, T.-M.; Stutz, S; Vaupel, A.; Jeay, S. (2016) [*Discovery of NVP-HDM201 – Identification of a Next-Generation Mdm2 inhibitor with superior characteristics.*](#) In: Annual Meeting of the ACS, 21-25 August, Philadelphia, PA, USA

Graphical abstract



15a
80 pM IC₅₀ MDM2 TR-FRET
11 nM GI₅₀ SJSA1 cell proliferation

Highlights

- Novel rationally designed p53-MDM2 inhibitor scaffold
- Structural proof of concept by x-ray crystallography
- Optimization of metabolic stability
- *In vivo* proof of concept with high efficacy